2024 IEEE/ASME International Conference on Advanced Intelligent Mechatronics (AIM)
July 15-19, 2024. Boston, MA, USA

Bounding Flight Control of Dynamic Morphing Wings

Bibek Gupta[1], Aniket Dhole[1], Adarsh Salagame[1], Xuejian Niu[1], Yizhe Xu[1], Kaushik Venkatesh[1], Paul Ghanem[1], Ioannis Mandralis[2], Eric Sihite[2], and Alireza Ramezani[1*]

***Abstract*— Vertebrate flyers perform intermittent flights as bounding or oscillating flights for power management. Intermittent flights and the resulting oscillating height during flapping and soaring provide the means of increasing speed without increasing flapping speed. These maneuvers and their robotic biomimicry have remained unexplored so far, which, if understood, can lead to aerial robot designs with endured flight operations. This works attempts to achieve robotic bounding flight using Northeastern's Aerobat platform. Aerobat can dynamically morph its wings by collapsing them rapidly during each gaitcycle. We present a launcher designed that allows bounding flight experimentation of Aerobat in a computer-aided fashion. We augmented Aerobat with a plural tiny thruster to stabilize its unstable roll, pitch, and yaw dynamics. This paper presents our control design based on extending Aerobat's states to accommodate unobservable aerodynamic forces and offers experimental results to support our proposed approach.**

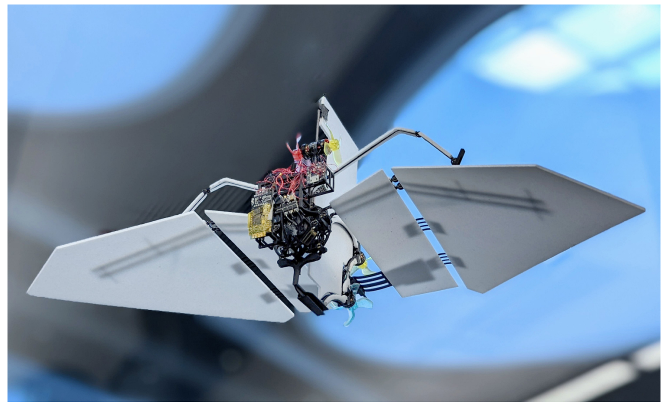

Fig. 1. Aerobat, a small flapping-wing, bioinspired bat robot with morphing wings.

I. Introduction

Vertebrate flyers perform intermittent flight in the form of bounding or oscillating flights for power management purposes [1]. Intermittent flights and the resulting oscillating height during flapping and soaring provide the means of increasing speed without increasing flapping speed [2]. Animal studies have remarkably covered flight endurance benefits of intermittent flight for a long time [3]–[5]. However, these maneuvers and their robotic biomimicry have remained unexplored so far. This works attempts to achieve robotic bounding flight using Northeastern's Aerobat platform.

Two scenarios can be considered in the intermittent flight of vertebrate flyers: 1) wings squeezed toward the body during some time interval during the flight, 2) wings kept straight with no plunge motions (soaring). Intermittent flight in both forms can enhance efficiency. The drag forces can be considered in profile (body) drag and trailing-vortex drags. The profile drag of the body remains the same during flapping and soaring. However, during flapping, particularly during the downstrokes, the wings experience large pressure gradients that negatively affect the formation of the boundary layer leading to significant drags. If we assume the trailing-vortex drags are proportional to the square of lift [6], during the downstrokes, which are the lift-thrust generating part of gait cycles, the trailing-vortex drags become larger [7]. So, downstrokes are energy hungry, and as a result, a natural approach chosen by vertebrate flyers is to minimize flapping cycles.

However, the total energy expenditure in undulating intermittent flights may remain similar to straight, continuous-flapping flights. The lift and lift-dependent drag forces in ascending and descending are less than from straight path flight (force and moment balance); however, in intermittent flights, a total amount of extra work is spent in other forms too. During the rise, extra energy is spent establishing the potential energy lost during descending. Therefore, the main advantage of intermittent flight comes from the significantly reduced rate of energy expenditure [8] which can help improve flight in small aerial robots.

Currently, lipo batteries are the only source of powering small aerial vehicles. The main reason for their popularity is their high energy density (very lightweight for the deliverable power), constant power output when discharging, and highest discharge rates, making them very suitable for energy-hungry multi-rotor systems. Suppose the principles of intermittent flight of vertebrate flyers are copied in aerial robots. In that case, other power source options with smaller discharge ratings with much longer operation times can be utilized with significant potential to augment operation times which currently do not exceed 10-15 min.

Note that bounding flights of Aerobat refer to its ability to squeeze its wings into the body dynamically and it differs from how biologists define bounding flight based on intermittent flaps. In this work, we briefly describe our attempt to achieve untethered outdoor flights with Aerobat platform shown in Fig. 1. This work is organized as follows. We briefly describe Aerobat's hardware and the launcher

[1]Authors are with the Silicon Synapse Labs, Department of Electrical and Computer Engineering, Northeastern University, Boston, USA. Emails: dhole.an, gupta.bi, salagame.a, a.ramezani@northeastern.edu

[2]Author is with the Department of Aerospace Engineering, California Institute of Technology, Pasadena, USA. Email: esihite@caltech.edu

*Corresponding author.

mechanism for our bounding flight. We present the dynamics of bounding flight and a closed-loop control for it. We report experimental validation of robotic bounding flight.

II. Hardware Concept

In this section, we briefly explain how Aerobat's bounding flights are achieved from a hardware design standpoint. In addition, we present the launcher platform designed to perform bounding flights successfully.

A. Aerobat's Computational Structures

The readers are referred to [9]–[12] for complete details about computational structures (see Fig. 3) used in Aerobat. However, for completeness of the work presented here, we briefly cover Aerobat's computational structure concept. To successfully develop a robotic wing structure that can expand and collapse during a gait cycle (approx. 100 msec), we considered the following design criterion:

- (a) a mechanical structure that mimics bats' DoF in a meaningful way,
- (b) a robust and flexible wing structure that facilitates control through morphological computation,
- (c) a small, lightweight, and compact mechanism that can undergo large external static and dynamic loads.

The biologically meaningful DoFs considered in Aerobat are the plunging motion and the wing extension/retraction, where the control is facilitated by changing the wing morphology or directly articulating the armwing kinetic sculpture. Using flexible joints to form a compliant structure, we mimic some of the natural bat wing's flexibility and the important DoFs for flapping flight packaged in a very compact mechanical structure.

The wing structure is articulated using a series of cranks and four-bar linkage mechanisms. This mechanism is actuated with only a single motor, therefore, the wing expansion/retraction is a slave to the flapping motion as it is actively actuated by the motor. Flexible joints are the core component of the wing's compliant mechanism, and several design considerations can be made which affect the hinge stiffness and robustness. There are several design variations for a compliant joint as outlined in [13], where they vary in size, off-axis stiffness, axis drift, stress concentration, and range of motion.

A softer and more flexible material has better compliance, so it can safely deform to counteract unexpected forces. However, it will also have worse resistance to torsion and off-axis perturbations. The planar four-bar linkage mechanism assumes the structure does not deform in the off-plane directions, so the low off-axis stiffness can be a significant issue. This problem can be addressed by using a larger cross-sectional area or by reinforcing the hinge with a flexible support structure post-fabrication to increase the off-axis stiffness of the hinge. The larger cross-sectional area increases the durability of the hinge but also increases the overall hinge stiffness and weight which is a design trade-off.

B. Active Pitch, Roll, and Passive Yaw Compensators

Our moment measurements using loadcell and analytical inspections inform that Aerobat is open-loop unstable in the sagittal, frontal, and transversal flight planes. We integrate three compensators into Aerobat's design to actively stabilize the bounding flight: two active roll and pitch stabilizers and one passive rudder-shape stabilizer (see Fig. 3). Witnessing longitudinal instability is not surprising from a tailless ornithopter. In addition, the moment measurements indicate that the robot is majorly pitch unstable. The pitching moment increases to up to 29 N.mm with an average value of 3.87 N.mm during the downstroke period. Further, by inspecting the roll and yaw moment measurements, we observed Aerobat is also unstable in the frontal and transversal planes of locomotion.

C. Launcher Design

We designed a launcher, shown in Fig. 2, to maintain consistent initial flight conditions in our untethered flight tests. The launcher comprises a launch rail, gripper assembly, release cam, and actuator assembly, which all sit on an off-the-shelf tripod. The actuator assembly, shown in Fig. 2, is custom-made and consists of a pancake brush-less DC motor, harmonic drive, incremental encoder, and ELMO power amplifier. The actuator assembly is torque-controlled using a PID controller to achieve desired launch speeds. It is energized with high-capacity LiPo batteries placed inside a safe box during outdoor untethered flights.

The gripper assembly is fixated on a timing belt pulled by a pulley attached to the actuator assembly. The spring-loaded gripper can reach up to 5 m/s linear speed along the launch rail. It opens when reaching the release cam. A follower mechanism, shown in Fig. 2, is designed as part of the gripper assembly to make the timely release of Aerobat possible.

III. Modeling

The modeling parameters used in this section are shown in Fig. 3. Consider the configuration variable vector q embodying underactuated (position and orientation) q_u and actuated wing coordinates q_a. After applying the Lagrange formalism, the dynamical equations of motion for the dynamic morphing robot is given by

$$D\ddot{q} + C\dot{q} + G = Bu + \left[\cdots J_i^\top \cdots\right] y + J_r^\top f_r + J_p^\top f_p \quad (1)$$

where D, C, and G are mass-inertia, Coriolis, and gravity matrices, respectively. In Eq., J_i, J_r, and J_p are the Jacobian matrices that project the external wing and compensator forces to the generalized coordinates q_i and are given by:

$$J_i = \frac{\partial p_i}{\partial \begin{bmatrix} q_u \\ q_a \end{bmatrix}} = \begin{bmatrix} \frac{\partial p_i}{\partial q_u} & \frac{\partial p_i}{\partial q_a} \end{bmatrix} \quad (2)$$

In Eq. 1, y denotes the output from the aerodynamic model, that is, the aerodynamic force. And, the compensator actions

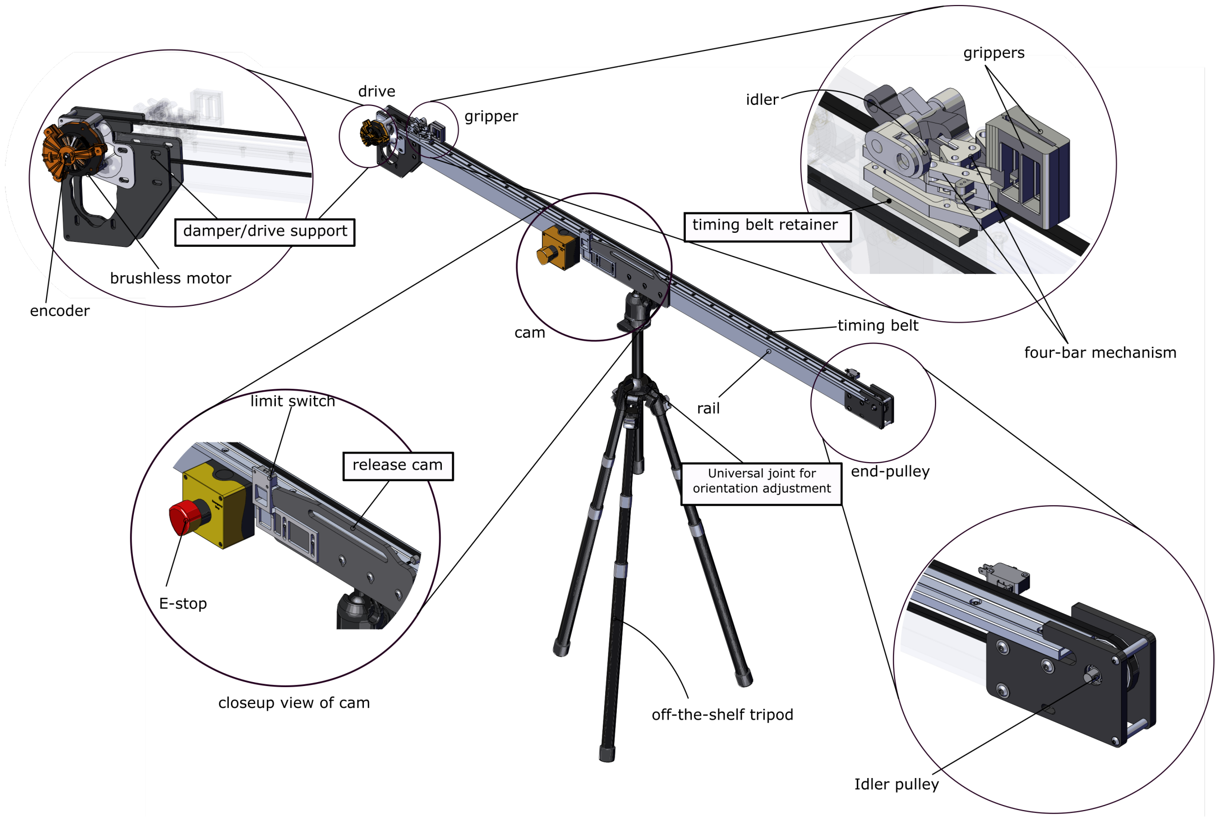

Fig. 2. Shows the custom launcher mechanism used to perform bounding flights. The launcher is motorized (far left) and can control the speed of the gripper during the launch phase. The orientation of the launch can be manually adjusted thanks to the universal joint that fixates the launcher to an off-the-shelf tripod.

are denoted by f_p and f_r (see Fig. 3). We partition the dynamics given by Eq. 1 as follows

$$\begin{bmatrix} D_u & D_{ua} \\ D_{au} & D_a \end{bmatrix} \begin{bmatrix} \ddot{q}_u \\ \ddot{q}_a \end{bmatrix} + \begin{bmatrix} H_u \\ H_a \end{bmatrix} = \begin{bmatrix} 0 \\ B_u \end{bmatrix} \tau + \sum_i \begin{bmatrix} J_{ui}^\top \\ J_{ai}^\top \end{bmatrix} y_i + \begin{bmatrix} J_{ur}^\top & J_{up}^\top \\ J_{ar}^\top & J_{ap}^\top \end{bmatrix} \begin{bmatrix} f_r \\ f_p \end{bmatrix} \tag{3}$$

We employ this partitioned dynamics to write the governing equations of motion for the position and orientation model, given by:

$$D_u \ddot{q}_u + D_{ua} \ddot{q}_a + H_u = J_1^* y + J_2^* u \tag{4}$$

where $J_1^* = \left[\dots J_{ui}^\top \dots \right]$ and $J_2^* = \left[J_{ur}^\top \; J_{up}^\top \right]$. This equation can be further simplified due to invertibility of D_u. As a result, we can write

$$\ddot{q}_u = -D_u^{-1} D_{ua} \ddot{q}_a - D_u^{-1} H_u + D_u^{-1} J_1^* y + D_u^{-1} J_2^* u \tag{5}$$

Last, the full-dynamics of the morphing model can be given by

$$\Sigma_{FullDyn} : \begin{cases} x_1 = \left[q_u^\top, \dot{q}_u^\top \right]^\top \\ \dot{x}_1 = x_2 \\ \dot{x}_2 = f + g_1 u + g_2 x_3 \\ \dot{x}_3 = G(t) \\ z = x_1 \end{cases} \tag{6}$$

where $f = -D_u^{-1} \Big(D_{ua} \ddot{q}_a - H_u \Big)$, $g_1 = D_u^{-1} J_2^*$. The model $\Sigma_{FullDyn}$ is extended with another state x_3 because

$$\Sigma_{AeroDyn} : \begin{cases} x_3 = y \\ g_2 x_3 = -\Big(D_u^{-1} J_1^* \Big) y \\ \dot{y} = \Pi_1(\xi)\xi + \Pi_2(\xi) a(t) \end{cases} \tag{7}$$

in this equation ξ and $a(t)$ are the aerodynamic model state vector and wing joint trajectories. Π_i denotes the aerodynamic model parameters. As this model suggests, technically the control design problem involves the closed-loop control of a multi-robot system (Aerobat and multi-rotor system) that interact with each other through an interconnected model while they possess little to no knowledge about each other's state information. Here the main objective is to use u in order to stabilize q_u and $\dot{q}_u$. For more details about how Eq. 7 is obtained, the reader is referred to [14], [15].

IV. Control

The control of Eq. 6 is considered here, assuming that u is calculated only based on $z = x_1$ observations. The time-varying term $G(t)$ is highly nonlinear; however, we have an efficient model of $G(t)$ [14]. We obtained an aerodynamic model in [14] that closely predicts the external aerodynamic forces impinged on Aerobat.

Using this model, we establish a state observer for x_3 to augment the feedback $u = K x_2$ (where K is the control

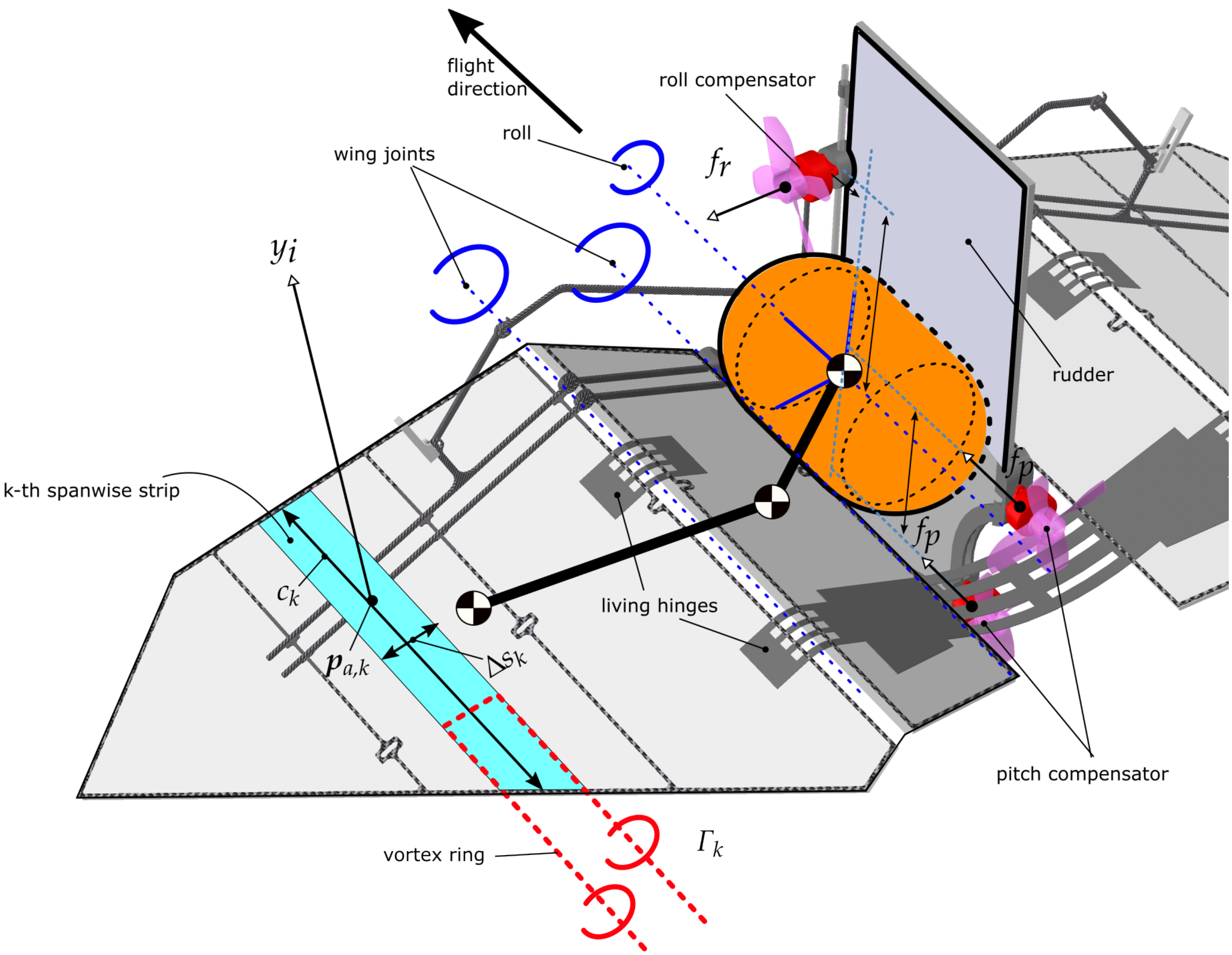

Fig. 3. Illustrates Aerobat's free-body-diagram with compensators and model parameters c_k (chord), Δs_k (span), and Γ_k (circulation) used to obtain y_i (aerodynamic force) at p_i on the wing. f_r and f_p are the roll- and pitch-compensating forces impinged on p_r and p_p, respectively.

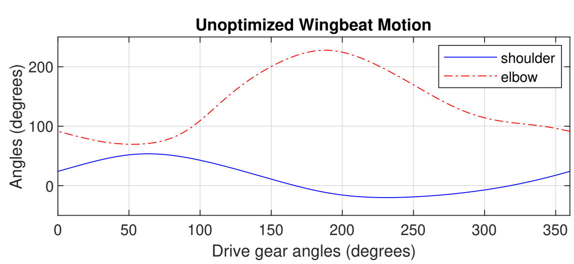

Fig. 4. Illustrates wing joint movements $a(t)$ (Fig. 3) from motion capture system.

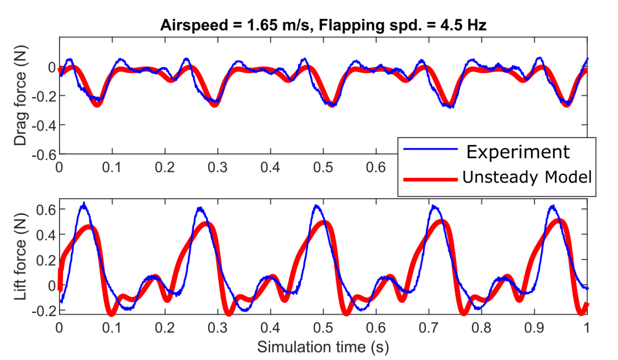

Fig. 5. Comparison between the experimental results and unsteady aerodynamic model predictions of drag and lift forces.

gain) so that $\dot{x}_2$ remains bounded and stable. Consider the following definition of estimated states $\hat{x}_i$:

$$\begin{aligned} \dot{\hat{x}}_1 &= \hat{x}_2 - \beta_1 \left(\hat{x}_1 - x_1\right) \\ \dot{\hat{x}}_2 &= f + g_1 u + g_2 \hat{x}_3 - \beta_2 \left(\hat{x}_1 - x_1\right) \\ \dot{\hat{x}}_3 &= -\beta_3 \left(\hat{x}_1 - x_1\right) \end{aligned} \tag{8}$$

where β_i is the observer gains. Now, we define the error $e_i = \hat{x}_i - x_1$ for $i = 1, 2, 3$. The following observer model is found

$$\begin{bmatrix} \dot{e}_1 \\ \dot{e}_2 \\ \dot{e}_3 \end{bmatrix} = \begin{bmatrix} -\beta_1 & I & 0 \\ -\beta_2 & 0 & g_2 \\ -\beta_3 & 0 & 0 \end{bmatrix} \begin{bmatrix} e_1 \\ e_2 \\ e_3 \end{bmatrix} + \begin{bmatrix} 0 \\ 0 \\ -I \end{bmatrix} G(t) \tag{9}$$

where I is identity matrix. The gains β_i for the observer

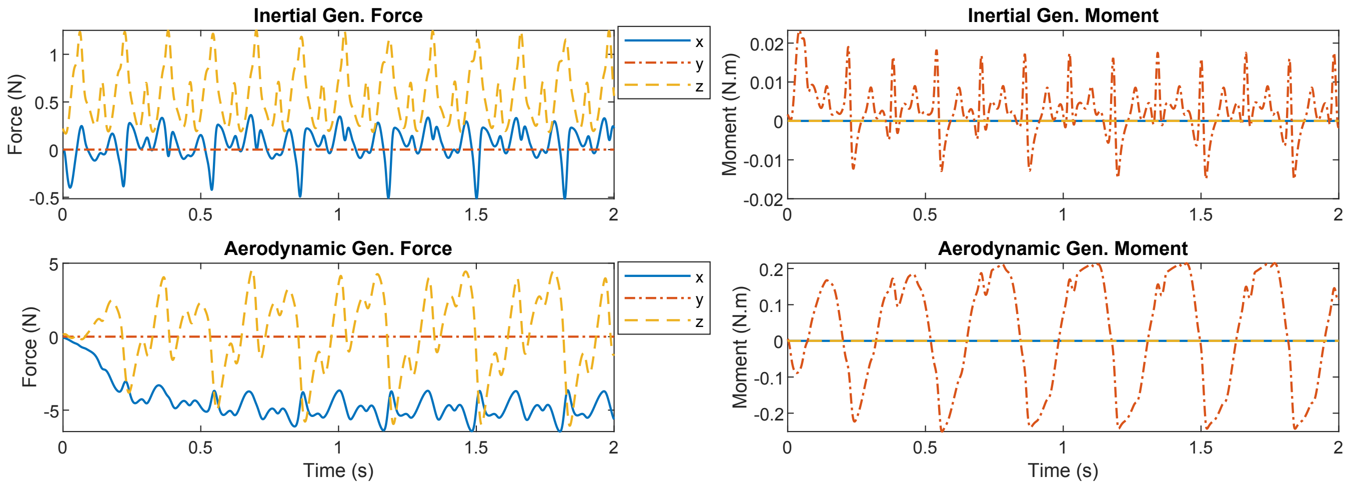

Fig. 6. Shows estimated generalized inertial $g_1^{-1}f$ and aerodynamics $g_1^{-1}g_2\hat{x}_3$ contributions based on knowledge on the boundedness of $\|g_2\|$ and $\|G(t)\|$ in Eq. 9.

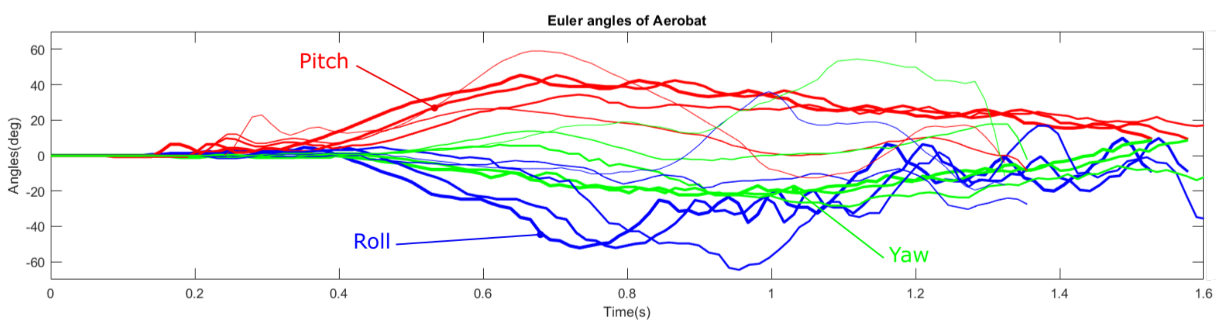

Fig. 7. Shows roll, pitch, yaw from several experiments.

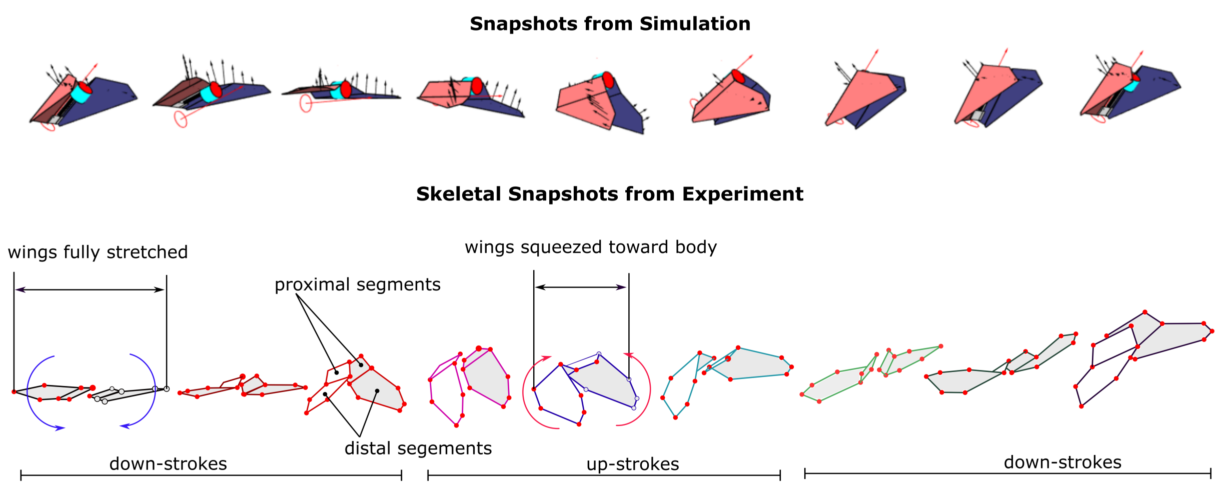

Fig. 8. Snapshots of experimental bounding flight and its comparison to simulated snapshots from Eq. 1

given by Eq. 9 can be obtained if upper bounds for G and g_2 can be assumed. We have extensively studied f, g_1 and g_2 terms in Aerobat's model in past and ongoing efforts. Based on the bounds for $\|f\|$, $\|g_1\|$, and $\|g_2\|$, we tuned the observer. The controller used for the bounding flight is given by

$$u = g_1^{-1}\Big(u_0 - f - g_2\hat{x}_3\Big) \tag{10}$$

where $u_0 = Kx_2$.

V. Results

As Eq. 10 suggests, the calculation of the control command $u = [f_r, f_p]^\top$ (roll and pitch compensators) relies on estimated values of the extended state x_3. The observers' performance explained in Eq. 9 highly depends on the characteristics of g_2 and $G(t)$. g_2 is the Jacobian term and we have complete knowledge about the boundaries of this term from p_r and p_p (see Fig. 3).

However, $G(t)$ has a complex form. Our unsteady aerodynamic model reported in [14] was used to identify the bounds on $G(t)$. The performance of this aerodynamic model for known wing trajectories (see Fig. 4) is shown in Fig. 5. Based on these results $\|G(t)\|$ was selected to estimate x_3. The estimated values $g_1^{-1}g_2\hat{x}_3$ denoted as generalized aerodynamic force contributions are shown in Fig. 6.

The estimated values $g_1^{-1}f$ shown in Fig. 6 and denoted as generalized inertial dynamics contributions were used to complete the computation of u. The observer given by Eq. 9 has a simple form and is calculated in real-time using Aerobat's onboard computer. The performance of the controller in stabilizing roll and pitch is shown in Fig. 7. Yaw is passively stabilized using the rudder shown in Fig. 3.

VI. Concluding Remarks

Vertebrate flyers perform intermittent flights as bounding or oscillating flights for power management. These maneuvers and their robotic biomimicry have remained unexplored so far, which, if understood, can lead to aerial robot designs with endured flight operations. In this paper, we reported robotic bounding flight using Northeastern's Aerobat platform. Aerobat can dynamically morph its wings by collapsing them rapidly during each gaitcycle. However, Aerobat's dynamic morphing poses serious flight control challenges. We designed a launcher that allows controlled flight initiation of Aerobat using a computer. In addition, we augmented Aerobat with a plural tiny thruster to stabilize its unstable roll, pitch, and yaw dynamics. A controller based on extending Aerobat's states to accommodate unobservable aerodynamic forces was designed. The controller was utilized to control bounding flights of Aerobat in the experiments that we conducted at Northeastern University.

References

[1] B. W. Tobalske, "Morphology, Velocity, and Intermittent Flight in Birds1," *American Zoologist*, vol. 41, no. 2, pp. 177–187, Apr. 2001.

[2] A. J. Ward-Smith, "Aerodynamic and energetic considerations relating to undulating and bounding flight in birds," *Journal of Theoretical Biology*, vol. 111, no. 2, pp. 407–417, Nov. 1984.

[3] D. K. Riskin, J. W. Bahlman, T. Y. Hubel, J. M. Ratcliffe, T. H. Kunz, and S. M. Swartz, "Bats go head-under-heels: The biomechanics of landing on a ceiling," *Journal of Experimental Biology*, vol. 212, no. 7, pp. 945–953, 2009.

[4] D. K. Riskin, A. Bergou, K. S. Breuer, and S. M. Swartz, "Upstroke wing flexion and the inertial cost of bat flight," *Proceedings of the Royal Society B: Biological Sciences*, vol. 279, no. 1740, pp. 2945–2950, 2012.

[5] J. Iriarte-Diaz, D. K. Riskin, D. J. Willis, K. S. Breuer, and S. M. Swartz, "Whole-body kinematics of a fruit bat reveal the influence of wing inertia on body accelerations," *Journal of Experimental Biology*, vol. 214, no. 9, pp. 1546–1553, 2011.

[6] F. T. Muijres, L. C. Johansson, R. Barfield, M. Wolf, G. R. Spedding, and A. Hedenström, "Leading-Edge Vortex Improves Lift in Slow-Flying Bats," *Science*, vol. 319, no. 5867, pp. 1250–1253, Feb. 2008.

[7] A. Hedenstrom and L. C. Johansson, "Bat flight: Aerodynamics, kinematics and flight morphology," *The Journal of experimental biology*, vol. 218, no. 5, pp. 653–663, 2015.

[8] J. Rayner, "Bounding and undulating flight in birds," *Journal of Theoretical Biology*, vol. 117, no. 1, pp. 47–77, 1985.

[9] E. Sihite, P. Kelly, and A. Ramezani, "Computational Structure Design of a Bio-Inspired Armwing Mechanism," *IEEE Robotics and Automation Letters*, vol. 5, no. 4, pp. 5929–5936, Oct. 2020.

[10] E. Sihite and A. Ramezani, "Enforcing nonholonomic constraints in Aerobat, a roosting flapping wing model," in *2020 59th IEEE Conference on Decision and Control (CDC)*, Dec. 2020, pp. 5321–5327.

[11] E. Sihite, A. Darabi, P. Dangol, A. Lessieur, and A. Ramezani, "An integrated mechanical intelligence and control approach towards flight control of aerobat," in *2021 American Control Conference (ACC)*, IEEE, 2021, pp. 84–91.

[12] A. Dhole, B. Gupta, A. Salagame, *et al.*, "Hovering control of flapping wings in tandem with multi-rotors," in *2023 IEEE/RSJ International Conference on Intelligent Robots and Systems (IROS)*, IEEE, 2023, pp. 6639–6644.

[13] B. P. Trease, Y.-M. Moon, and S. Kota, "Design of Large-Displacement Compliant Joints," *Journal of Mechanical Design*, vol. 127, no. 4, pp. 788–798, Nov. 2004.

[14] E. Sihite, P. Ghanem, A. Salagame, and A. Ramezani, "Unsteady aerodynamic modeling of aerobat using lifting line theory and wagner's function," in *2022 IEEE/RSJ International Conference on Intelligent Robots and Systems (IROS)*, IEEE, 2022, pp. 10 493–10 500.

[15] E. Sihite, A. Salagame, P. Ghanem, and A. Ramezani, "Actuation and flight control of high-dof dynamic morphing wing flight by shifting structure response," in *2023 62nd IEEE Conference on Decision and Control (CDC)*, IEEE, 2023, pp. 8824–8829.